Case Studies in Thermal Engineering 45 (2023) 103008

Contents lists available at ScienceDirect

Case Studies in Thermal Engineering

journal homepage: www.elsevier.com/locate/csite

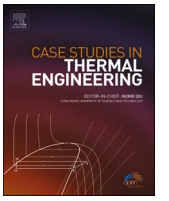

Significance of viscous dissipation, nanoparticles, and Joule heat on the dynamics of water: The case of two porous orthogonal disk

Qadeer Raza [a,b,1], M Zubair Akbar Qureshi [b], Shalan Alkarni [c], Bagh Ali [d], Ali Zain [e], Kanayo Kenneth Asogwa [f], Nehad Ali Shah [g,1], Se-Jin Yook [h,*]

[a] School of Mathematics and Statistics, Xi'an Key Laboratory of Scientific Computation and Applied Statistics, Northwestern Polytechnical University, Xi'an, 710129, China
[b] Department of Mathematics, Air University, Islamabad, Multan, 60000, Pakistan
[c] Department of Mathematics, College of Sciences, King Saud University, P.O.Box 2455, Riyadh, 11451, Saudi Arabia
[d] Faculty of Computer Science and Information Technology, Superior University, Lahore, 54000, Pakistan
[e] Department of Mathematics, National College of Business Administration and Economics, Lahore, Multan, Pakistan
[f] Department of Mathematics, Nigeria Maritime University, Okerenkoko, Delta State, Nigeria
[g] Department of Mechanical Engineering, Sejong University, Seoul, 05006, Republic of Korea
[h] School of Mechanical Engineering, Hanyang University, 222 Wangsimni-ro, Seongdong-gu, Seoul, 04763, Republic of Korea

ARTICLE INFO

Handling Editor: Huihe Qiu

Keywords:
Viscous dissipation and Joule heating
Hybrid nanofluid
Porous disk

ABSTRACT

This research explores the association between the Viscous dissipation and joule heat effect for hybrid-nanofluids (HN_{fd}) flow across absorbent surfaces. Expanding/contracting geometry with permeable factor advanced work for (HN_{fd}), which are accumulated of Silver (Ag-Metallic) and copper (Cu-Metallic). The flow passes through the orthogonally moving porous disks with a magnetic field. Comparison and critical study of the bottom and top porous surfaces of the discs are also shown here. Comparability transformations, the prime PDEs of the current model are transformed into high-order nonlinear ODEs, which are subsequently resolved numerically using the "Shooting Method." As discussed graphically the characterization of the flow, and thermal are demonstrated in detail, while the numerical result calculate in the upper and lower porous disk of a physical parameter such as skin friction coefficient (C_f) and Nusselt number (Nu) at lower and upper disks are respectively discussed.

1. Introduction

Viscous dissipation is the process by which the mechanical energy of a fluid is converted into heat due to internal frictional forces. This phenomenon is important in high-speed fluid flows, as it can significantly affect the temperature distribution and overall energy balance of the system. In contrast, Joule heating is the process by which electrical energy is converted into heat when an electric current flows through a conductor. This is an important consideration in systems that involve the flow of electrically conducting fluids, such as liquid metal cooling systems in nuclear reactors. Both of these phenomena have numerous applications in various fields, including heat exchangers, lubrication of mechanical systems, and electronic cooling systems. Understanding the effects of viscous dissipation and Joule heating (VD&JH) is critical in optimizing the performance of such systems. Most investigators also did some work

* Corresponding author.
E-mail addresses: shalkarni@ksu.edu.sa (S. Alkarni), nehadali199@sejong.ac.kr (N.A. Shah), ysjnuri@hanyang.ac.kr (S.-J. Yook).
[1] These authors contributed equally to this work and are co-first authors.

https://doi.org/10.1016/j.csite.2023.103008
Received 21 February 2023; Received in revised form 1 April 2023; Accepted 12 April 2023
Available online 13 April 2023
2214-157X/© 2023 The Authors. Published by Elsevier Ltd. This is an open access article under the CC BY-NC-ND license (http://creativecommons.org/licenses/by-nc-nd/4.0/).

considering the heating impact of viscous dissipation and joule. For instance, Hayat [1] Sequential impacts of viscous dissipation and Joule flow insulation have been evaluated using vertical porous revolving disks. Consideration is provided to radiative flow saturating porous space. For the situation of strong, suction that is uniform, Borisevich [2] studied the flow of heat transfer time-dependent moving disk in such a velocity electric field. With a (VD&JH) allowance, the temperature transfer rate at the disc surface is monitored in proportion to the magnetic field's amplitude and the rotational speed of the disks. The impacts of VD&JH combined with stable MHD are examined in OSALUSI [3], as well as the slip-flow of the electricity conducted incompressible viscous non-Newtonian Bingham liquid across porosity spinning disks. Iqbal [4] investigated the heat and mass transfer across 2 orthogonally rotating permeable coaxial disks, together with the impacts of suction and viscous dissipation, in an unsteady hydromagnetic viscosity electrically transmitting incompressible liquid (N_{fd}) (including titanium dioxide NPs). Hayat [5] this paper aims at studying second-grade nano liquid flow through a revolving disk. (N_{fd}) is heavily dependent upon Brownian motion and thermophoresis under investigation. Energy transfer under dissipation and Joule heating are studied. Chamkha [6] the researchers are studying the thermal boundary layer and MHD flow of (HN_{fd}) among double surfaces in a rotating both porous surface.Reddy [7] existence of heat transfer characteristics, for laminar nanoparticle concentration and temperature transformation a 2-D mathematical analysis of thermally conducting, viscous, and Joule (Ohmic) heat source across an able adsorption a porous surface. The impacts of heating from the thermal radiation and Joule are considered. Khader [8] experiment was carried out to look into the consequences of continuous thermal conduction on Newtonian fluid flow and energy transmission through a constantly growing porous layer, (VD&JH), MHD, and current radioactivity.

Currently, due to its comprehensive technological, Production, and research purposes such as exchange, Micronutrition, Medical fabrication, Cooling motor, acoustics protection, naval constructions, solar heating, and lubricating, among other things Engineers, scientists, and researchers have responded positively to a new group of active thermal effective fluids known as HN_{fd}. Hybrid nanofluids are a type of engineered fluids that combine 2 kinds of NPs in a base fluid (size smaller than 100 nm) [9,10]. They possess enhanced thermal conductivity, electrical conductivity, and mechanical properties, making them useful in applications such as electronics cooling, energy storage, and biomedical engineering. In electronics cooling, hybrid nanofluids can improve heat transfer rates, leading to better device performance and reliability. In energy storage, hybrid nanofluids can be used to improve the thermal management of energy storage systems, resulting in increased efficiency and longer lifespan. In biomedical engineering, they have potential applications in drug delivery, tissue engineering, and medical imaging. Due to spinning discs, Xu [11] unsteady combined convective of a (HN_{fd}) is investigated. To model, the problem is developed the generalized uniformly system of flow which explains (HN_{fd}) comprising multiple types of NPs. Nilankush [12] literature displays Hall existing features over a spinning disk on (HN_{fd}) flow. This also included the impacts of heat particles and the magnetosphere to research the fine points of the flow. (N_{fd}) flow across flexible retardation moving disks was demonstrated by Fang and Tao [13]. Here, he gave unstable viscous fluid flow some thought. Turkyilmazoglu [14] researched the heat transfer of nano liquid passing through a spinning disc. Yin [15] investigated the heat transfer of (N_{fd}) on a rotating disc that is being stretched radially. In the study by Ashwini [16], laminar, incompressible, and 2-D micropolar liquid stream among permeable disks is taken into account. Ghaffar [17] investigated inviscid unstable laminar fluid movement among two orthogonally traveling coaxial disks is called quantitatively. The goal of this work, according to Behnam [18], is to semi-analytically examine when a (SiC–TiO2/DO) (HN_{fd}) flows across porosity revolving disks that are visible to a continuous vertical magnetic field.Hayat [19] addressed the flux of thermal radiation and nonlinear convection of silver and copper water nano liquids. Kumar [20] produced in-situ copper-zinc (Cu–Zn) hybrid NPs for temperature profile, standard cutting fluids are employed. Qureshi [21] investigated the flow of heat transfer in MHD, unsteady, serval shape and size factor, different types of NP's effect in permeable coaxial disks in magnetized (HN_{fd}) flow. The impact of various magnetized 3D nanomaterials on the liquid flow among two orthogonal spinning discs was examined by Abdulmalek [22]. Bachok [23] examined the movement of a (N_{fd}) across spinning permeable disks in terms of thermal transmission. Qureshi [24] looked into the temperature and mass transfer evaluation of a non-Newtonian fluid flow across permeable sides when magnetic nanoparticles were present. Bilal [25] conducted the numerical methods of magnetic and metallic NP's in porous materials utilizing the Darcy-Forchheimer correlation. Gangadhar [26] conducted a numerical analysis of thermal transfer (HN_{fd}) with two different magnetic and metallic NP's (MgO–Au) and base fluid water used. Bhargavi [27] considered both linear and nonlinear thermal radiation effects when investigating the thermal transport of the flow. Several researchers have conducted numerical analyses of hybrid nanofluids, as evidenced by studies cited in Refs. [28–36]·

Magnetohydrodynamics, in which polar rises a flowing conducting fluid, describes its flow characteristics. Magnetic field influences are investigated in a variety of industrial processes, including fuel manufacture, electrical generators, crystal creation, nuclear power plants, and aerodynamics. Alfven [37] created the MHD field. A hybrid magnetized nanocomposite in a permeable stretched solution has been given a numerical treatment by Emad [38]. Chamkha [39] premeditated the impact of MHD (N_{fd}) convective thermal transmission on heat radiation utilizing the regulated volume-based. Dogonchi and Ganji [40] investigated the models for temperature distribution in an axially symmetric tube with porous walls for a non-Newtonian flowing fluid for turbine cooling systems. Krishna [41] investigated the thermal performance of aluminum oxide and copper nanofluids moving in a steady MHD flow via an extended porosity layer. Devi and Devi [42] investigated the MHD flow of heat transfer in (HN_{fd}) of movable porous surfaces from metallic (Cu) and non-metallic (Al_2O_3) nanoparticles are used with the base fluid water. Krishna [43] has recently been investigated at radiative MHD Casson (HN_{fd}) flow through a massively enhanced perpendicular porous medium. MHD flow investigated by many researchers Ref [44–59].

This study's main objective is to examine the effects of joule heating and viscous dissipation on the 2-D HN_{fd} the flow of thermal transfer among two orthogonally moving porous disks. As previously stated, there has been no research on the analysis of metallics used by NP's dispersion to measure thermal conductivity within fluid areas. As a result, the main objective of this article is to examine the flow of heat transfer of metallic hybrid nanofluid (Ag–Cu/H_2O) behavior graphically in velocity and temperature profiles.

Considering governing PDEs, the dimensionless ordinary differential equations (ODEs) model is developed. The architecture of the ODEs was mathematically computed by the 4th-RK integration approach and the "shooting technique." Tables and graphs are used to investigate the physical variable data.

2. Mathematical formulation

Consider a 2-D hybrid MHD nanofluid flow that is Time-dependent, laminar, incompressible, and contains (Ag–Cu/water) NP's among two orthogonally movable permeable coaxial disks under the influence of viscous dissipation and joule heating with permeability in the existence of a magnetic field that is generated with amplitude in the z-direction. The boundary disks of diameter **2r**, upward and downward with uniform velocity $l(t)$ and are at a variable distance 2 $l(t)$. Based on the assumption that the Reynolds number is minimal, the produced magnetic field is disregarded. The liquid has a velocity distribution of v=(u(r, z, t),0, w(r, z, t)) show in Fig. 1. The law of conservation of mass, momentum, and energy has the following form for the aforementioned problem Ref [60]:

$$\frac{\partial u}{\partial r}+\frac{u}{r}+\frac{\partial w}{\partial z}=0 \tag{1}$$

$$\frac{\partial u}{\partial t}+\mathrm{u}\,\frac{\partial u}{\partial r}+\mathrm{w}\,\frac{\partial u}{\partial z}=-\frac{1}{\rho_{hnf}}\,\frac{\partial p}{\partial r}+\upsilon_{hnf}\left(\frac{\partial^2 u}{\partial r^2}+\frac{1}{r}\,\frac{\partial u}{\partial r}-\frac{u}{r^2}+\frac{\partial^2 u}{\partial z^2}\right)-\frac{\sigma_e B_0^2}{\rho_{hnf}}u \tag{2}$$

$$\frac{\partial w}{\partial t}+\mathrm{u}\,\frac{\partial w}{\partial r}+\mathrm{w}\,\frac{\partial w}{\partial z}=-\frac{1}{\rho_{nf}}\,\frac{\partial p}{\partial z}+\upsilon_{hnf}\left(\frac{\partial^2 w}{\partial r^2}+\frac{1}{r}\,\frac{\partial w}{\partial r}+\frac{\partial^2 w}{\partial z^2}\right) \tag{3}$$

$$\frac{\partial T}{\partial t}+\mathrm{u}\,\frac{\partial T}{\partial r}+\mathrm{w}\,\frac{\partial T}{\partial z}=\alpha_{hnf}\frac{\partial^2 T}{\partial z^2}+\frac{\mu_{hnf}}{(\rho c)_{p\,hnf}}\left(\frac{\partial u}{\partial z}\right)^2+\frac{\sigma_e B_0^2\,u^2}{(\rho c_p)_{hnf}} \tag{4}$$

Where B_0^2 stand for magnetic field, p, σ_e, T represented by pressure, electrical conductivity Pressure and temperature, while α_{hnf},ρ_{hnf} and υ_{hnf} show the thermal diffusivity, density, and υ_{hnf} is its kinematic viscosity of HN_{fd} .

$$\upsilon_{hnf}=\frac{\mu_{hnf}}{\rho_{hnf}}\ \text{ and }\alpha_{hnf}=\frac{k_{hnf}}{(\rho c_p)_{hnf}},Pr=\frac{(\mu C_p)_{bf}}{k_{bf}} \tag{5}$$

Here solid and liquid NP's density is demonstrated by ρ_s, and ρ_f. Furthermore, specific heat capacity, dynamic viscosity and thermal conductivity of HN_{fd} are denoted by $(\rho c_p)_{hnf}$, μ_{hnf} and k_{hnf}.

The flow situation for boundary conditions are:

$$z_1=-l(t)\quad u=0\quad w=-A_1 l'(t)\quad \mathrm{T}=T_1\quad \text{and}$$

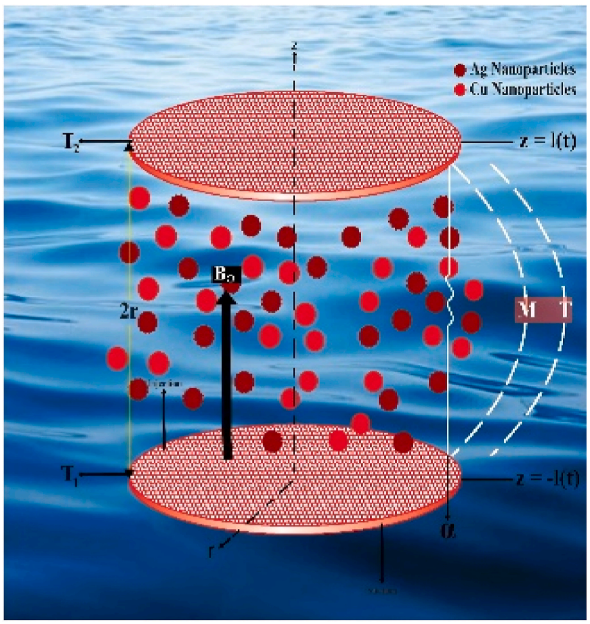

Fig. 1. Physical model.

$$z_1 = l(t) \quad u = 0 \quad w = A_1 l'(t) \quad \mathrm{T} = T_2 \tag{6}$$

The dash represents the derivative for time t, and A_1 is the measurement of split porosity.
Similarity transformations (7) apply to above equations (1)–(4) and remove the pressure term.

$$\eta = \frac{z}{l} \quad \mathrm{u} = -\frac{r\upsilon_f}{l} F_\eta(\eta, t) \quad \mathrm{w} = \frac{2\upsilon_f}{l} F(\eta, t) \quad \theta = \frac{T - T_2}{T_1 - T_2}, \tag{7}$$

and result

$$\frac{\upsilon_{hnf}}{\upsilon_f} F_{\eta\eta\eta\eta} + \alpha(3F_{\eta\eta} + \eta F_{\eta\eta\eta}) - 2FF_{\eta\eta\eta} - \frac{a^2}{\upsilon_f} - \frac{\rho_f}{\rho_{hnf}} \mathrm{M}\, F_{\eta\eta} = 0 \tag{8}$$

$$\theta_{\eta\eta} + \frac{\upsilon_f}{\alpha_{hnf}} (\alpha\eta - 2F)\theta_\eta + [(1-\varphi)^{-2.5} {F_\eta}^2 + M{F_\eta}^2] E_c P_r \frac{\kappa_f}{\kappa_{hnf}} - \frac{a^2}{\alpha_{nf}} \theta_t = 0 \tag{9}$$

Using the boundary condition

$$\eta = -1, F = -Re, F_\eta = 0, \theta = 1,$$

$$\text{and } \eta = 1, F = Re, F_\eta = 0, \theta = 0. \tag{10}$$

The bottom and top disk are constant temperatures T_1 and T_2 (with $T_1 > T_2$) (with T_1 greater than T_2)respectively, $\alpha = \frac{l l'(t)}{\upsilon_f}$ is the wall expansion ratio, $Re = \frac{A_1 l l'(t)}{2\upsilon_f}$ is the absorptivity Reynolds number , $M = \frac{\sigma_e B_0^2 l^2}{\mu_{hnf}}$ is the magnetic parameter, $P_r = \frac{(\mu c_p)_f}{\kappa_f}$ is the Prandtl number and the Eckert number is denoted by $E_c = \frac{U^2}{(T_1 - T_2)(\rho c_p)_f}$.

Putting $F = f\,Re$ in the above equations (8) and (9) and investigating the described by Majdalani [61] where α is a constant, $f = f(\eta)$, and $\theta = \theta(\eta)$, as a result of which $\theta_t = 0$ and $f_{\eta\eta t} = 0$. As a result, we obtain the following equations.

$$\frac{\upsilon_{hnf}}{\upsilon_f} f_{\eta\eta\eta\eta} + \alpha(3f_{\eta\eta} + \eta f_{\eta\eta\eta}) - 2Reff_{\eta\eta\eta} - \frac{\rho_f}{\rho_{hnf}} \mathrm{M}\, f_{\eta\eta} = 0 \tag{11}$$

$$\theta_{\eta\eta} + \frac{\upsilon_f}{\alpha_{hnf}} Pr(\alpha\eta - 2Ref)\theta_\eta + \left[(1-\varphi)^{-2.5} {f_{\eta\eta}}^2 + M{f_\eta}^2\right] E_c P_r \frac{\kappa_f}{\kappa_{hnf}} = 0 \tag{12}$$

$$\eta = -1;\ f = -1, f_\eta = 0, \theta = 1, \text{and}$$

$$\eta = 1;\ f = 1, f_\eta = 0, \theta = 0.$$

3. Practical and engineering interests

3.1. Skin friction coefficients (C_f)

$C_{f(\eta=1)}$ and $C_{f(\eta=-1)}$ denoted for both porous disks, which are given as

$$C_{f(\eta=-1)} = \frac{\xi_{zr}|_{z=-k}}{\rho_f (l' A_1)^2} = \frac{1}{Re_r (1 - \varphi_1 - \varphi_2)^{2.5}} f''(-1), \tag{13}$$

$$C_{f(\eta=1)} = \frac{\xi_{zr}|_{z=k}}{\rho_f (l' A_1)^2} = \frac{1}{Re_r (1 - \varphi_1 - \varphi_2)^{2.5}} f''(1)$$

Where $Re_r = 4\left(\frac{l}{r}\right)\left(\frac{1}{Re}\right)^2$ represent for local Reynolds number, and ξ_{zr} are shear stresses in the radial direction at the bottom and upper disk are express as

$$\xi_{zr} = \mu_{hnf} \left(\frac{\partial u}{\partial z}\right)|_{z=-k} = \frac{\mu_{bf}}{(1 - \varphi_1 - \varphi_2)^{2.5}} \left(\frac{r\upsilon_f}{l^3}\right) f''(-1)$$

$$\xi_{zr} = \mu_{hnf} \left(\frac{\partial u}{\partial z}\right)|_{z=k} = \frac{\mu_{bf}}{(1 - \varphi_1 - \varphi_2)^{2.5}} \left(\frac{r\upsilon_f}{l^3}\right) f''(1)$$

4. Nusselt numbers

The heat transmission rate is calculated at the bottom and top disk (Nusselt numbers) Nu_{z-1} and Nu_{z1} are given as

$$Nu|_{z=1} = \frac{ls_z}{\kappa_f(T_1 - T_2)}|_{z=-k} = -\frac{k_{hnf}}{k_f}\theta'(-1)$$

$$Nu|_{z=-1} = \frac{ls_z}{\kappa_f(T_1 - T_2)}|_{z=k} = -\frac{k_{hnf}}{k_f}\theta'(1) \tag{14}$$

Where Here heat flux is denoted as s_z which follows as,

$$s_z|_{z=-k} = -k_{hnf}\left(\frac{\partial T}{\partial z}\right)|_{z=-k} = -\frac{(T_1 - T_2)}{l}k_{hnf}\theta'(-1)$$

$$s_z|_{z=k} = -k_{hnf}\left(\frac{\partial T}{\partial z}\right)|_{z=k} = -\frac{(T_1 - T_2)}{l}k_{hnf}\theta'(1)$$

5. Result and discussion

The numerical computing process produces graphical representations (2–6) that illustrate the effects of α, $Re, M,\ \varphi_1, \varphi_2\ Pr,$ and Ec on the velocity and temperature profiles of the fluid. Table 1 provides an in-depth analysis of the thermophysical properties of the hybrid nanofluid (HN_{fd}), while Table 2 presents the characteristics of the base fluid and metallic NPs. Table 3 displays that the values of the expansion ratio parameter (α) are greater than zero. This results in a reduction in the flow of shear stress and heat transfer in both the Ag-water and Cu-water cases. However, the values of the Re increase, and as a result, the flow of f''(−1) and θ′(−1) are enhanced. A much better numerical outcome is measured in Cu-water as compared to Ag-water for the lower porous disk. Moreover, magnetic parameter and volume friction are greater than zero, then the shear stress and flow of heat transfer act vice versa in both cases. If we increase the values of the expansion ratio parameter α in the hybrid nanofluid of the lower porous disk shown in Table 4, the flow of shear stress and thermal transfer is reduced. On the other hand, if we enhance the values of the Reynolds number Re, the shear stress and flow of heat transfer rate are increased. However, if we increase the values of the magnetic parameter, the volume of friction M, and both φ_1 and φ_2, the shear stress and flow of heat transfer act opposite in the lower porous disk. Upon comparing Tables 3 and 4, we analyzed that the numerical accuracy of shear stress is much better in the nanofluid (Cu-Water). However, the flow of thermal conductivity is much better in the hybrid nanofluid (Ag–Cu/water). Table 5 displays that the expanding/contracting α increases the values of φ_1 and φ_2 effect shear stress and heat transfer flow in metallic (HN_{fd}) (Ag–Cu/water). While thermal transmission and shear force flow (measured as the Nusselt number) is increased in situations of contraction, they are decreased in circumstances of lower disc expansion. Table 6 demonstrated that the permeable Re is effect expansion ratio varies from -ve to + ve in thermal transmission and shear force decreases in lower disks. Table 7 demonstrates that when the Re and M values are less than zero, shear force and the rate of thermal transference rise, but when these values are more than zero, the impact of decreased disc momentum and the rate of thermal transfer is lessened. In a metallic (HN_{fd}), Table 8 displays the impact of several dimensions on the C_f and Nu for each porosity disk. Furthermore, the C_f and Nu rise with increasing values of the permeability $, M,\ \varphi_1$ *and* φ_2, while they decrease with increasing values of the α, $Pr,$ and Ec in either permeable disk. Before visualizing the results, we cross-checked our findings with previously published research papers using Table 7. As demonstrated in Fig. 2(a) and 3(a), the α fluctuates between negative and positive values, increasing the volume friction impact of the A_{VP}. The thickness of the center of the barrier velocity porous medium increases as the disk size increases. as seen in Fig. 2(a) and 3(a). Figs. 2(b) and 3(b) showed that the R_{VP} had a greater impact on the φ_1, φ_2 and α than the center of the wall layer, but less of an impact on the thickness of the velocity porous medium. Fluid motion is symmetrically drawn. Fig. 2(c) and 3(c) presented there are decreased thermal boundary layer thicknesses for T_P in expanding/contracting expansion ratio and increased values of volume friction. Because this temperature inversion impact is considered, the efficient thermal variation throughout the layer and the external fluid is minimized, resulting in less temperature. Physically, the volume friction parameter (φ_1, φ_2) for nanoparticles refers to the resistance experienced by the fluid flow due to the presence of the nanoparticles within the porous disk. The value of this parameter for the first and second nanoparticles can have a significant impact on the overall flow dynamics and heat transfer characteristics of system. A higher value of this parameter indicates greater resistance to fluid flow and can result in reduced heat transfer rates. The influence of the M on the A_{VP} and R_{VP} was seen in Fig. 4(a) and (b). As the M strength increases, the thickness of the velocity porous medium also reduces in the A_{VP}, but it grows in the wall domain where the R_{VP} is lower. The application of a transverse magnetic field orthogonal to the flow direction produces a drag force called the Lorentz force, which attempts to resist the liquid motion and so reduce its velocity. Fig. 5 shows that the effect of Pr for T_P impact of fixed parameter $\alpha = 5, Re = 1, \varphi_1 = \varphi_2 = 0.05, Ec = 0.00068, M = 1$. Increases values of Pr than thermal boundary layer are increases. Physically, the Prandtl number is an important parameter in porous disk systems as it determines the efficiency of heat transfer relative to the momentum transfer. A higher Prandtl number implies that the fluid has a lower capacity to transfer heat compared to momentum, and

Table 1
Thermophysical properties of (HN_{fd}).

Title H_2 O (f) $Ag(\varphi_1)$ Cu (φ_2)	
ρ(kg m^{-3})	997.0 19 300 8933
C_p (J k $g^{-1}k^{-1}$)	4180 129 385
$\kappa(wm^{-1}k^{-1})$	0.6071 317 400

Table 2
Density (ρ_{hnf}), viscosity (μ_{hnf}), Heat Capacity $(\rho c_p)_{hnf}$, and Thermal Conductivity (k_{hnf}) Hybrid nanofluid thermophysical properties.

Properties	Hybrid Nanofluid (Ag–Cu-water)
Density (ρ)	$\rho_{hnf} = \varphi_1\rho_{s_1} + \varphi_2\rho_{s_2} - (1 - \varphi_1 - \varphi_2)\,\rho_{bf}$
Viscosity (μ)	$\mu_{hnf} = \frac{\mu_{bf}}{(1-\varphi_1-\varphi_2)^{2.5}}$
Heat Capacity (ρC_P)	$(\rho c_p)_{hnf} = \varphi_1(\rho c_p)_{s_1} + \varphi_2(\rho c_{p_)} + (1 - \varphi_1 - \varphi_2)\,(\rho c_p)_{bf}$
Thermal Conductivity (K)	$k_{hnf} = \frac{k_{s2} + (N-1)k_{nf} - (N-1)\varphi_2(k_{nf} - k_{s2})}{k_{s2} + (N-1)k_{nf} + \varphi_2(k_{nf} - k_{s2})}k_{nf}$ Where $k_{nf} = \frac{k_{s1} + (N-1)k_{bf} - (N-1)\varphi_1(k_{bf} - k_{s1})}{k_{s1} + (N-1)k_{bf} + \varphi_1(k_{bf} - k_{s1})}k_{bf}$

Table 3
Numerical impact of serval parameter in shear stress ($f''(-1)$) and heat transfer $\theta'(-1)$ for different Nanofluids (Ag-water) and (Cu-water).

				Ag-water		Cu-water	
α	Re	M	φ	$\lvert f''(-1)\rvert$	$\lvert\theta'(-1)\rvert$	$\lvert f''(-1)\rvert$	$\lvert\theta'(-1)\rvert$
0.3	0.1	2	0.02	3.1308	0.44407	3.1664	0.44365
0.6				2.8308	0.23988	2.9120	0.23874
0.9				2.5383	0.12309	2.6629	0.12197
1.2				2.2537	0.06072	2.4194	0.05987
0.3	0.2			3.2017	0.69172	3.2270	0.69238
	0.3			3.2772	1.0213	3.2909	1.02391
	0.4			3.3574	1.4271	3.358	1.43261
	0.2	4		3.4750	0.44234	3.5081	0.44194
		6		3.7898	0.44084	3.8208	0.44045
		8		4.0806	0.43952	4.1101	0.43914
		2	0.03	3.09671	0.44596	3.14905	0.44536
			0.04	3.06415	0.44778	3.13239	0.44701
			0.05	3.03293	0.44952	3.11639	0.44859

Table 4
Numerical values for Hybrid Nanofluids impact on Shear Stress and Nusselt Number (heat transfer).

					Ag–Cu/water	
α	Re	M	φ_1	φ_2	$\lvert f''(-1)\rvert$	$\lvert\theta'(-1)\rvert$
0.3	0.1	2	0.02	0.02	3.0983	0.44745
0.6					2.7797	0.2515
0.9					2.4694	0.13501
1.2					2.1681	0.05988
0.3	0.2				3.17301	0.67901
	0.3				3.2527 1	0.98319
	0.4				3.3377	1.3555
	0.1	4			3.4285	0.44586
		6			3.7315	0.44448
		8			4.012	0.44326
		2	0.03		3.0664	0.44922
			0.04		3.0359	0.45093
			0.05		3.0067	0.45256
			0.02	0.03	3.0831	0.44904
				0.04	3.0685	0.45057
				0.05	3.0546	0.45204

vice versa. This parameter significantly impacts the flow behavior and heat transfer characteristics of the system. Fig. 6 indicates that when the Ec in the T_P for α and Re are higher than zero, the temperature boundary layer thickness rises in the center of the wall and both permeable disks. The Eckert number is a dimensionless quantity that characterizes the relative strength of thermal energy and kinetic energy in a fluid. In the context of a porous disk system, it determines the amount of thermal energy that is converted into kinetic energy due to the presence of the disk. This parameter plays a critical role in determining the heat transfer rate and flow behavior of the system, particularly in high-speed flow regimes. A higher Eckert number indicates that kinetic energy dominates over thermal energy, and vice versa for a lower Eckert number (see Table 9).

Table 5
Expanding/contractions impact of volume fraction for $Re = -1, Pr = 6.2, M = 1, Sc = 0.00068$.

$\varphi_1 = \varphi_2$	$\alpha = 2$		$\alpha = -2$	
	$\lvert f''(-1)\rvert$	$\lvert \theta'(-1)\rvert$	$\lvert f''(-1)\rvert$	$\lvert \theta'(-1)\rvert$
0.01 = 1%	1.5144769	0.0004847451	4.2231765	0.2264021
0.02 = 2%	1.3868956	0.0004411569	4.3458779	0.241936
0.03 = 3%	1.2943281	0.0004128910	4.4490523	0.256353
0.04 = 4%	1.2265624	0.0003924690	4.5350458	0.2697399
0.05 = 5%	1.17650773	0.0003728408	4.6057507	0.2821776

Table 6
Expanding/contractions effect of permeable Reynold number for $\varphi_1 = \varphi_2 = 0.02, Pr = 6.2, Ec = 0.00068, M = 1$.

α	$Re = 1$		$Re = -1$	
	$\lvert f''(-1)\rvert$	$\lvert \theta'(-1)\rvert$	$\lvert f''(-1)\rvert$	$\lvert \theta'(-1)\rvert$
−2	7.09276800	153.6655	4.3458779	0.2419364
−1	5.65462238	7.997268	3.4385043	0.0174583
0	4.20163944	3.424350	2.6366499	0.0008259
1	2.7238269	2.541335	1.9512178	0.0009660
2	1.1937794	0.985217	1.3868956	0.0004411

Table 7
Permeable Reynold number effect of magnetic parameter for $\varphi = 0.02, Pr = 6.2, Ec = 0.00068, M = 1$.

M	$Re = -1$		$Re = 1$	
	$\lvert f''(-1)\rvert$	$\lvert \theta'(-1)\rvert$	$\lvert f''(-1)\rvert$	$\lvert \theta'(-1)\rvert$
1	4.34587793	0.2419364	7.09276800	153.665571
2	4.46768005	0.2429469	6.96600219	273.059920
3	4.58621101	0.2437763	6.66310461	329.410934
4	4.70168846	0.2444371	6.41950094	362.840044
5	4.81430907	0.2449402	5.55019746	269.463363

6. Conclusion

The study investigates the heat transfer characteristics of a metallic HN_{fd} (Cu–Ag/H_2O) in a 2-dimensional, time-dependent, Viscous dissipation and joual heating effect flow. The fluid flow occurs between orthogonally moving porous coaxial disks and comprises MHD, and Newtonian fluids, with water as the base fluid. Two different types of metallic NPs are used for this purpose. The study examines the impact of several non-dimensional parameters, such as Re, Ec, Pr, α φ_1 and φ_2 on the temperature profile and velocity profile of the fluid flow. The results of the study, including the shear stress, skin friction coefficient, Nusselt number, and comparison of the flow of heat transfer in nanofluid and hybrid nanofluid, are presented both graphically and numerically. The following are the study's key findings:

- An increase in the values of the expanding/contraction ratio parameter α results in a reduction of the flow of skin friction coefficient and Nusselt number in the lower porous disk for the HN_{fd} (Cu–Ag/H_2O).
- Increasing the volume fraction of the first and second nanoparticles results in an increase in the momentum boundary layer thickness at the middle of the wall. However, there is a decrease in the boundary layer thickness in both porous disks along the radial velocity profile.
- If we increase the values of the Eckert number and Prandtl number, the thermal boundary layer thickness will also increase on the temperature profile in both porous disks.
- Augmenting the values of the M leads to an augmentation in the momentum boundary layer thickness in both permeable disks for the radial velocity profile.
- The numerical analysis indicates that the shear stress flow is significantly better in the nanofluid (Cu-Water), while the thermal conductivity is higher in the HN_{fd}.
- Enhancing the values of the Permeable Reynolds number results in a rise in both the shear stress flow and heat transfer rate in the lower porous disk.

Author statement

All authors contributed equally to this work.

Table 8
Numerical compute the impact of different nano dimensional parameters on the C_f and the Nu.

α	Re	M	φ_1	φ_2	Pr	Ec	$\lvert C_f \rvert$	$\lvert Nu \rvert$
−2	−1	1	0.01	0.01	6.2	0.00068	4.223176	0.2264021
−1							3.418333	0.0128129
0							2.693457	0.0013296
1							2.057089	0.0010392
2							1.514476	0.0004847
−2	−1	1	0.01	0.01	6.2	0.00068	3.418333	0.0128129
	−0.5						3.745685	0.3406023
	0						4.158208	0.2563534
	0.5						4.666706	0.2697399
	1						5.277397	0.2821776
−2	−1	1	0.01	0.01	6.2	0.00068	3.418333	0.0128129
		3					3.690268	0.0127519
		5					3.946125	0.0125918
		7					4.188123	0.0123441
		9					4.418055	0.0120187
−2	−1	1	0.01	0.01	6.2	0.00068	4.223176	0.2264021
			0.02				4.322086	0.2354093
			0.03				4.412592	0.2439744
			0.04				4.495423	0.2521268
			0.05				4.571203	0.2598936
−2	−1	1	0.01	0.01	6.2	0.00068	4.223176	0.2264021
				0.02			4.251841	0.2331789
				0.03			4.277908	0.2397446
				0.04			4.301496	0.2461054
				0.05			4.322714	0.2522677
−2	−1	1	0.01	0.01	5.5	0.00068	4.2231765	0.2503563
					5.9		4.2231765	0.2364647
					6.2		4.2231765	0.2264021
					6.5		4.2231765	0.2166398
					7.7		4.2231765	0.2102962
−2	−1	1	0.01	0.01	6.2	0.00051	4.2231765	0.2297354
						0.00055	4.2231765	0.2289511
						0.00060	4.2231765	0.2279707
						0.00064	4.2231765	0.2271864
						0.00068	4.2231765	0.2264021

Table 9
Presents a comparative analysis of the $f''(-1)$ and $\theta'(-1)$ flow at the lower disk for fixed parameter values of $\alpha = 2, Re = -10, \varphi_1 = \varphi_2 = 0.1$.

M	Ali et al. [60]		Present Results	
	$\lvert f''(-1) \rvert$	$\lvert \theta'(-1) \rvert$	$\lvert f''(-1) \rvert$	$\lvert \theta'(-1) \rvert$
0	1.8580	2.9180	1.8582	2.9182
2	1.9009	3.0519	1.9011	3.0521
4	1.9439	3.1893	1.9441	3.1895
6	1.9871	3.3300	1.9873	3.3302
8	2.0303	3.4740	2.0305	3.4742

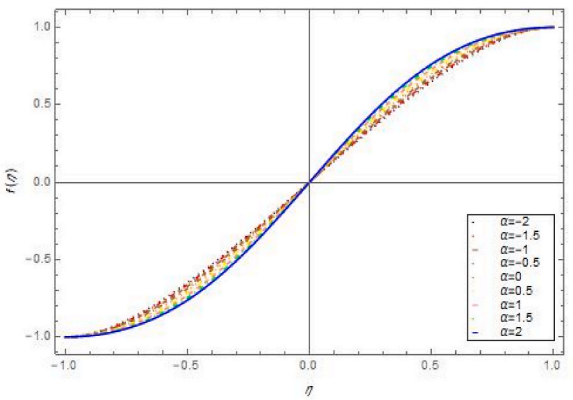

Fig. 2(a). Influence in A_{VP} of α for $\varphi_1 = \varphi_2 = 0.01, Re = -1, M = 1, Ec = 0.00068, Pr = 6.2$.

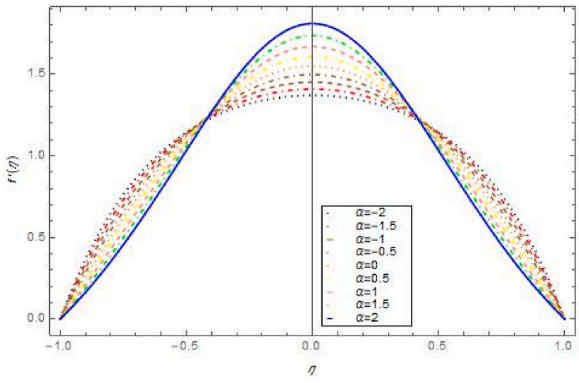

Fig. 2(b). Influence in R_{VP} of α for $\varphi_1 = \varphi_2 = 0.01, Re = -1, M = 1, Ec = 0.00068, Pr = 6.2$.

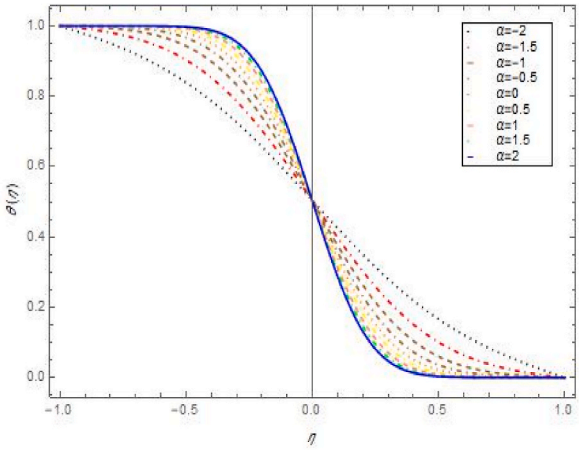

Fig. 2(c). Influence in T_P of α for $\varphi_1 = \varphi_2 = 0.01, Re = -1, M = 1, Ec = 0.00068, Pr = 6.2$.

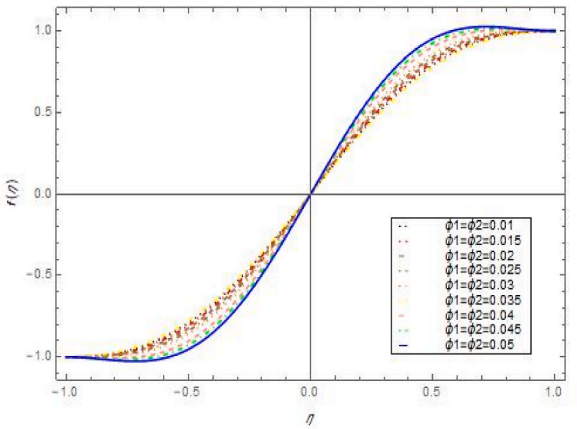

Fig. 3(a). Influence in A_{VP} of volume fraction for $= 2, Re = 2, M = 1, Ec = 0.00068, Pr = 6.2$.

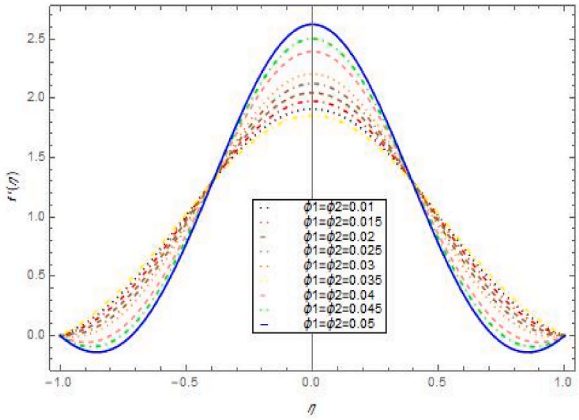

Fig. 3(b). Influence in R_{VP} of volume fraction for $\alpha = 2$, $Re = 2, M = 1, Ec = 0.00068, Pr = 6.2$.

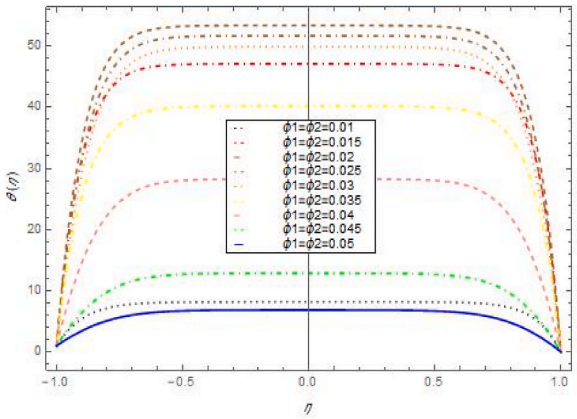

Fig. 3(c). Influence in T_P of volume fraction for $\alpha = 2$, $Re = 2, M = 1, Ec = 0.00068, Pr = 6.2$.

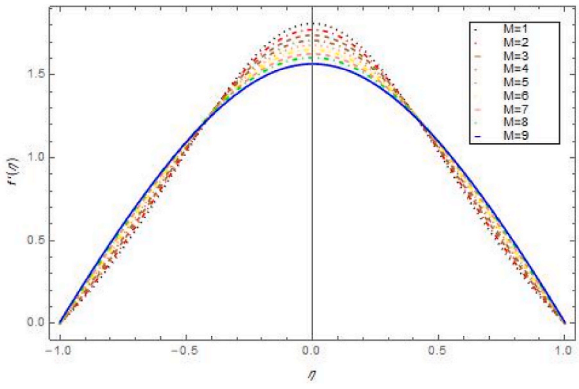

Fig. 4(a). Influence in R_{VP} of M for $= 1$, $Re = -1, \varphi_1 = \varphi_2 = 0.01, Ec = 0.00068, Pr = 6.2$.

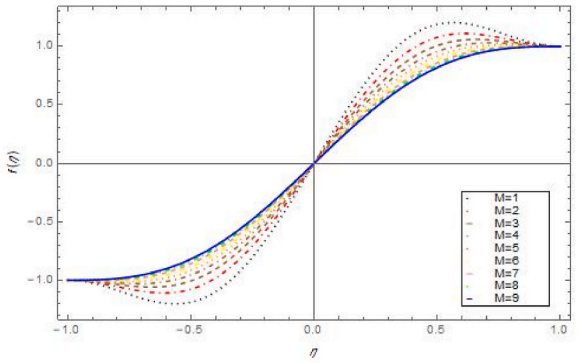

Fig. 4(b). Influence in A_{VP} of M for $= 1$, $Re = -1, \varphi_1 = \varphi_2 = 0.01, Ec = 0.00068, Pr = 6.2$.

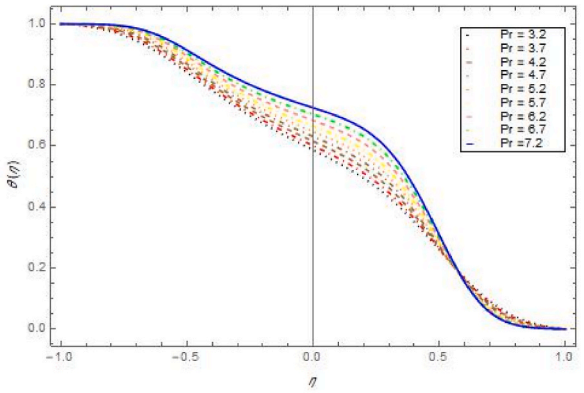

Fig. 5. Influence in T_P of Pr for $\alpha = 5$, $Re = 1, \varphi_1 = \varphi_2 = 0.05, Ec = 0.00068, M = 1$.

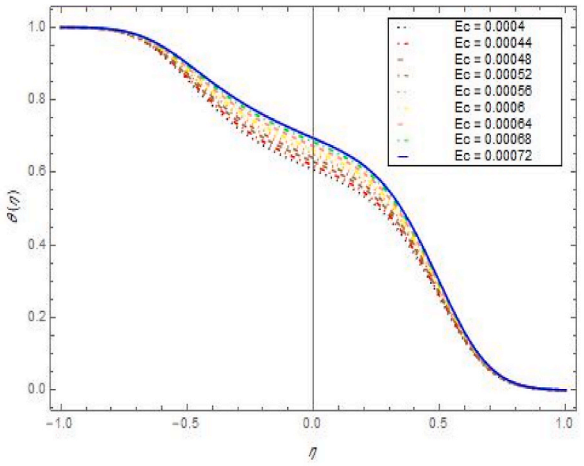

Fig. 6. Influence in T_P of Ec for $\alpha = 5$, $Re = 1, \varphi_1 = \varphi_2 = 0.03$, M = 1, $Pr = 6.2$.

Declaration of competing interest

The authors declare that they have no known competing financial interests or personal relationships that could have appeared to influence the work reported in this paper.

Data availability

Data will be made available on request.

Nomenclature

B_o	Uniform magnetic field [T]
C_f	skin friction coefficient
C_p	Specific heat at constant pressure
k	Dimensionless parameter
M	Magnetic parameter
Pr	Prandtl number
r z	Cylindrical coordinates system
Re	Reynolds number
w	Mass or velocity component along z axis [gr or m/s]
Nu	Nusselt number
ρ_{hnf}	density for (HN_{fd})
ρ_{s2}	density for second solid NP's
k_{s1}	Thermal conductivity for first solid fraction
k_{mbf}	thermal conductivity for shape base fluid
k_{bf}	thermal conductivity for base fluid
μ_{bf}	viscosity base fluid
F_η	The dimensionless radial velocity profile
θ_η	Dimensionless temperature profile
σ	Electrical conductivity [(m^3A^2)/kg]
υ	Kinematic viscosity [m^2/s]
μDynamic viscosity [P_a.s]ρ	Dynamic viscosity [P_a.s]ρDensity [kg/ m^3]
ρC_P	Volumetric heat capacity [J/(m3 K)]
T	Temperature [K]
$(\rho c_p)_{hnf}$	specific heat capacity for (HN_{fd})
ρ_{s1}	density for first solid NP's
k_{hnf}	Thermal conductivity for (HN_{fd})
k_{s2}	Thermal conductivity for second solid fraction
p	Pressure
Ec	Eckert number
υ_{hnf}	kinematics viscosity for (HN_{fd})

Subscripts

(b_{fd})	base fluid
(HN_{fd})	Hybrid Nanofluid
1	First nanoparticle(Ag)
A_{VP}	Axial Velocity profile
T_P	Temperature Profile
(N_{fd})	Nanofluid
2	second nanoparticle (Cu)
R_{VP}	Redial velocity profile

Greek symbols

α	Thermal diffusivity [m^2/s]
φ	Equivalent nanoparticles volume fraction
φ_1	The equivalent first nanoparticles volume fraction
η	Independent similarity variable
φ_2	The equivalent first nanoparticles volume fraction

References

[1] T. Hayat, M. Imtiaz, A. Alsaedi, Melting heat transfer in the MHD flow of Cu–water nanofluid with viscous dissipation and Joule heating, Adv. Powder Technol. 27 (4) (2016 Jul 1) 1301–1308.

[2] V.D. Borisevich, E.P. Potanin, Effects of viscous dissipation and Joule heat on heat transfer near a rotating disk in the presence of intensive suction, J. Eng. Phys. 55 (5) (1988 Nov) 1220–1223.

[3] Emmanuel Osalusi, Jonathan Side, Robert Harris, Barry Johnston, in: On the Effectiveness of Viscous Dissipation and Joule Heating on Steady MHD Flow and Heat Transfer of a Bingham Fluid over a Porous Rotating Disk in the Presence of Hall and Ion-Slip Currents, vol. 34, 2007, pp. 1030–1040, 9-10.

[4] M.F. Iqbal, K. Ali, M. Ashraf, Heat and mass transfer analysis in unsteady titanium dioxide nanofluid between two orthogonally moving porous coaxial disks: a numerical study, Can. J. Phys. 93 (3) (2015) 290–299.
[5] T. Hayat, S. Qayyum, M.I. Khan, A. Alsaedi, Entropy generation in magnetohydrodynamic radiative flow due to rotating disk in presence of viscous dissipation and Joule heating, Phys. Fluids 30 (1) (2018 Jan 3), 017101.
[6] J. Chamkha Ali, A.S. Dogonchi, D.D. Ganji, Magneto-hydrodynamic flow and heat transfer of a hybrid nanofluid in a rotating system among two surfaces in the presence of thermal radiation and Joule heating, AIP Adv. 9 (2) (2019), 025103, https://doi.org/10.1063/1.5086247.
[7] M.G. Reddy, Effects of Thermophoresis, viscous dissipation and Joule heating on steady MHD flow over an inclined radiative isothermal permeable surface with variable thermal conductivity, J. Appl. Fluid Mech. 7 (1) (2014 Jan 1) 51–61.
[8] M.M. Khader, Fourth-order predictor-corrector FDM for the effect of viscous dissipation and Joule heating on the Newtonian fluid flow, Comput. Fluids 182 (2019 Mar 30) 9–14.
[9] H.R. Ashorynejad, A. Shahriari, MHD natural convection of hybrid nanofluid in an open wavy cavity, Results Phys. 9 (2018 Jun 1) 440–455.
[10] M. Hassan, M. Marin, R. Ellahi, S.Z. Alamri, Exploration of convective heat transfer and flow characteristics synthesis by Cu–Ag/water hybrid-nanofluids, Heat Tran. Res. 49 (18) (2018).
[11] H. Xu, Modelling unsteady mixed convection of a nanofluid suspended with multiple kinds of nanoparticles between two rotating disks by generalized hybrid model, Int. Commun. Heat Mass Tran. 108 (2019 Nov 1), 104275.
[12] N. Acharya, R. Bag, P.K. Kundu, Influence of Hall current on radiative nanofluid flow over a spinning disk: a hybrid approach, Phys. E Low-dimens. Syst. Nanostruct. 111 (2019 Jul 1) 103–112.
[13] T. Fang, H. Tao, Unsteady viscous flow over a rotating stretchable disk with deceleration, Commun. Nonlinear Sci. Numer. Simul. 17 (12) (2012) 5064–5072.
[14] M. Turkyilmazoglu, Nanofluid flow and heat transfer due to a rotating disk, Comput. Fluid 94 (1) (2014) 139–146.
[15] C. Yin, L. Zheng, C. Zhang, X. Zhang, Flow and heat transfer of nanofluids over a rotating disk with uniform stretching rate in the radial direction, Propul. Power Res. 6 (1) (2017 Mar 1) 25–30.
[16] A. Bhat, N.N. Katagi, Micropolar fluid flow between a non-porous disk and a porous disk with slip: Keller-box solution, Ain Shams Eng. J. 11 (1) (2020 Mar 1) 149–159.
[17] M. Ghaffar, K. Ali, A. Yasmin, M. Ashraf, Unsteady flow between two orthogonally moving porous disks, J. Mech. 31 (2) (2015 Apr) 147–151.
[18] B. Fallah, S. Dinarvand, M. Eftekhari Yazdi, M.N. Rostami, I. Pop, MHD flow and heat transfer of SiC-TiO2/DO hybrid nanofluid due to a permeable spinning disk by a novel algorithm, J. Appl. Computat. Mech. 5 (5) (2019 Oct 1) 976–988.
[19] T. Hayat, S. Qayyum, M. Imtiaz, A. Alsaedi, Comparative study of silver and copper water nanofluids with mixed convection and nonlinear thermal radiation, Int. J. Heat Mass Tran. 102 (2016 Nov 1) 723–732.
[20] M.S. Kumar, V. Vasu, A.V. Gopal, Thermal conductivity and rheological studies for Cu–Zn hybrid nanofluids with various basefluids, J. Taiwan Inst. Chem. Eng. 66 (2016 Sep 1) 321–327.
[21] M. Qureshi, S. Bilal, M.Y. Malik, Q. Raza, E.S. Sherif, Y.M. Li, Dispersion of metallic/ceramic matrix nanocomposite material through porous surfaces in magnetized hybrid nanofluids flow with shape and size effects, Sci. Rep. 11 (1) (2021 Jun 10) 1–9.
[22] Z. Abdelmalek, M.Z. Qureshi, S. Bilal, Q. Raza, E.S. Sherif, A case study on morphological aspects of distinct magnetized 3D hybrid nanoparticles on fluid flow between two orthogonal rotating disks: an application of thermal energy systems, Case Stud. Therm. Eng. 23 (2021 Feb 1), 100744.
[23] N. Bachok, A. Ishak, I. Pop, Flow and heat transfer over a rotating porous disk in a nanofluid, Phys. B Condens. Matter 406 (9) (2011 Apr 15) 1767–1772.
[24] M.Z. Qureshi, K. Ali, M.F. Iqbal, M. Ashraf, Heat and mass transfer analysis of unsteady non-Newtonian fluid flow between porous surfaces in the presence of magnetic nanoparticles, J. Porous Media 20 (12) (2017).
[25] S. Bilal, M. Qureshi, Mathematical analysis of hybridized ferromagnetic nanofluid with induction of copper oxide nanoparticles in permeable channel by incorporating Darcy–Forchheimer relation, Mathemat. Sci. (2021 Jul 15) 1–7.
[26] K. Gangadhar, R. Edukondala Nayak, M. Venkata Subba Rao, T. Kannan, Nodal/Saddle stagnation point slip flow of an aqueous convectional magnesium oxide–gold hybrid nanofluid with viscous dissipation, Arabian J. Sci. Eng. 46 (2021 Mar) 2701–2710.
[27] D.N. Bhargavi, K. Gangadhar, A.J. Chamkha, Graphene-gold/PDMS Maxwell hybrid nanofluidic flow in a squeezed channel with linear and irregular radiations, Proc. IME E J. Process Mech. Eng. (2022 Nov 20), 09544089221139696.
[28] K. Gangadhar, M.A. Kumari, A.J. Chamkha, EMHD flow of radiative second-grade nanofluid over a Riga Plate due to convective heating: revised Buongiorno's nanofluid model, Arabian J. Sci. Eng. 47 (7) (2022 Jul) 8093–8103.
[29] K. Gangadhar, M.A. Kumari, M. Venkata Subba Rao, A.J. Chamkha, Oldroyd-B nanoliquid flow through a triple stratified medium submerged with gyrotactic bioconvection and nonlinear radiations, Arabian J. Sci. Eng. (2022 Jul 1) 1–3.
[30] G. Kotha, V.R. Kolipaula, M. Venkata Subba Rao, S. Penki, A.J. Chamkha, Internal heat generation on bioconvection of an MHD nanofluid flow due to gyrotactic microorganisms, European Phys. J. Plus 135 (2020 Jul) 1–9.
[31] K. Gangadhar, K. Bhanu Lakshmi, T. Kannan, A.J. Chamkha, Bioconvective magnetized oldroyd-B nanofluid flow in the presence of Joule heating with gyrotactic microorganisms, Waves Random Complex Media (2022 Mar 17) 1–21.
[32] K. Gangadhar, A.J. Chamkha, Entropy minimization on magnetized Boussinesq couple stress fluid with non-uniform heat generation, Phys. Scripta 96 (9) (2021 Jun 3), 095205.
[33] K. Gangadhar, P. Manasa Seshakumari, M. Venkata Subba Rao, A.J. Chamkha, Biconvective transport of magnetized couple stress fluid over a radiative paraboloid of revolution, Proc. IME E J. Process Mech. Eng. 236 (4) (2022 Aug) 1661–1670.
[34] K. Gangadhar, R. Edukondala Nayak, M. Venkata Subba Rao, A.J. Chamkha, Nonlinear radiations in chemically reactive Walter's B nanoliquid flow through a rotating cone, Proc. IME E J. Process Mech. Eng. (2022 Jun 21), 09544089221105932.
[35] K. Gangadhar, K. Bhanu Lakshmi, S. El-Sapa, M. Venkata Subba Rao, A.J. Chamkha, Thermal energy transport of radioactive nanofluid flow submerged with microorganisms with zero mass flux condition, Waves Random Complex Media (2022 May 12) 1–23.
[36] K. Gangadhar, E. Mary Victoria, A.J. Chamkha, Hydrothermal features in the swirling flow of radiated graphene–Fe3O4 hybrid nanofluids through a rotating cylinder with exponential space-dependent heat generation, Waves Random Complex Media (2022 Jul 20) 1–24.
[37] H. Elfven, Existence of electromagnetic hydrodynamic waves, Nature 150 (1942) 405–406.
[38] E.H. Aly, I. Pop, MHD flow and heat transfer over a permeable stretching/shrinking sheet in a hybrid nanofluid with a convective boundary condition, Int. J. Numer. Methods Heat Fluid Flow (2019 Aug 15).
[39] A.J. Chamkha, A.S. Dogonchi, D.D. Ganji, Magnetohydrodynamic nanofluid natural convection in a cavity under thermal radiation and shape factor of nanoparticles impacts: a numerical study using CVFEM, Appl. Sci. 8 (12) (2018 Nov 26) 2396.
[40] A.S. Dogonchi, D.D. Ganji, Investigation of heat transfer for cooling turbine disks with a non-Newtonian fluid flow using DRA, Case Stud. Therm. Eng. 6 (2015 Sep 1) 40–51.
[41] M. Veera Krishna, Heat transport on steady MHD flow of copper and alumina nanofluids past a stretching porous surface, Heat Transfer 49 (3) (2020 May) 1374–1385.
[42] S.A. Devi, S.S. Devi, Numerical investigation of hydromagnetic hybrid Cu–Al2O3/water nanofluid flow over a permeable stretching sheet with suction, Int. J. Nonlinear Sci. Numer. Stimul. 17 (5) (2016 Aug 1) 249–257.
[43] M.V. Krishna, N.A. Ahammad, A.J. Chamkha, Radiative MHD flow of Casson hybrid nanofluid over an infinite exponentially accelerated vertical porous surface, Case Stud. Therm. Eng. 27 (2021 Oct 1), 101229.
[44] S.M. Murshed, K.C. Leong, C. Yang, Investigations of thermal conductivity and viscosity of nanofluids, Int. J. Therm. Sci. 47 (5) (2008 May 1) 560–568.
[45] S.R. Yan, A.H. Pordanjani, S. Aghakhani, A.S. Goldanlou, M. Afrand, Managment of natural convection of nanofluids inside a square enclosure by different nano powder shapes in presence of Fins with different shapes and magnetic field effect, Adv. Powder Technol. 31 (7) (2020 Jul 1) 2759–2777.
[46] Q. Raza, M.Z. Qureshi, B.A. Khan, A. Kadhim Hussein, B. Ali, N.A. Shah, J.D. Chung, Insight into dynamic of mono and hybrid nanofluids subject to binary chemical reaction, activation energy, and magnetic field through the porous surfaces, Mathematics 10 (16) (2022 Aug 21) 3013.

[47] S. Anitha, T. Thomas, V. Parthiban, M. Pichumani, What dominates heat transfer performance of hybrid nanofluid in single pass shell and tube heat exchanger? Adv. Powder Technol. 30 (12) (2019 Dec 1) 3107–3117.
[48] G. Rasool, N.A. Ahammad, M.R. Ali, N.A. Shah, X. Wang, A. Shafiq, A. Wakif, Hydrothermal and mass aspects of MHD non-Darcian convective flows of radiating thixotropic nanofluids nearby a horizontal stretchable surface: passive control strategy, Case Stud. Therm. Eng. 42 (2023), 102654.
[49] I. Kazemi, M. Sefid, M. Afrand, A novel comparative experimental study on rheological behavior of mono & hybrid nanofluids concerned graphene and silica nano-powders: characterization, stability and viscosity measurements, Powder Technol. 366 (2020 Apr 15) 216–229.
[50] A. Moradi, M. Zareh, M. Afrand, M. Khayat, Effects of temperature and volume concentration on thermal conductivity of TiO2-MWCNTs (70-30)/EG-water hybrid nano-fluid, Powder Technol. 362 (2020 Feb 15) 578–585.
[51] I. Waini, A. Ishak, I. Pop, Hybrid nanofluid flow and heat transfer over a nonlinear permeable stretching/shrinking surface, Int. J. Numer. Methods Heat Fluid Flow (2019 Jun 4).
[52] Q. Raza, M.Z. Qureshi, B. Ali, A.K. Hussein, B.A. Khan, N.A. Shah, W. Weera, Morphology of hybrid MHD nanofluid flow through orthogonal coaxial porous disks, Mathematics 10 (18) (2022 Sep 9) 3280.
[53] A. Abderrahmane, N.A.A. Qasem, O. Younis, R. Marzouki, A. Mourad, N.A. Shah, J.D. Chung, MHD hybrid nanofluid mixed convection heat transfer and entropy generation in a 3-D triangular porous cavity with Zigzag wall and rotating cylinder, Mathematics 10 (5) (2022) 769.
[54] N.A. Shah, A. Ebaid, T. Oreyeni, S.-J. Yook, MHD and Porous Effects on Free Convection Flow of Viscous Fluid between Vertical Parallel Plates: Advance Thermal Analysis, Waves in Random and Complex Media, 2023, https://doi.org/10.1080/17455030.2023.2186717.
[55] K. Sajjan, N.A. Shah, N.A. Ahammad, C.S.K. Raju, M.D. Kumar, W. Weera, Nonlinear Boussinesq and Rosseland approximations on 3D flow in an interruption of Ternary nanoparticles with various shapes of densities and conductivity properties, AIMS Mathematics 7 (10) (2022) 18416–18449.
[56] P. Priyadharshini, M.V. Archana, N.A. Ahmmad, C.S. K Raju, S.-J. Yook, N.A. Shah, Gradient descent machine learning regression for MHD flow: metallurgy process, Int. Commun. Heat Mass Tran. 138 (2022), 106307.
[57] Q. Lou, B. Ali, S.U. Rehman, D. Habib, S. Abdal, N.A. Shah, J.D. Chung, Micropolar dusty fluid: coriolis force effects on dynamics of MHD rotating fluid when Lorentz force is significant, Mathematics 10 (15) (2022 Jul 27) 2630.
[58] M.Z. Ashraf, S.U. Rehman, S. Farid, A.K. Hussein, B. Ali, N.A. Shah, W. Weera, Insight into significance of bioconvection on mhd tangent hyperbolic nanofluid flow of irregular thickness across a slender elastic surface, Mathematics 10 (15) (2022 Jul 25) 2592.
[59] M.Z. Qureshi, M. Faisal, Q. Raza, B. Ali, T. Botmart, N.A. Shah, M.Z. Qureshi, M. Faisal, Q. Raza, B. Ali, Morphological nanolayer impact on hybrid nanofluids flow due to dispersion of polymer/CNT matrix nanocomposite material, AIMS Math 8 (1) (2023) 633–656.
[60] K. Ali, M.Z. Akbar, M.F. Iqbal, M. Ashraf, Numerical simulation of heat and mass transfer in unsteady nanofluid between two orthogonally moving porous coaxial disks, AIP Adv. 4 (10) (2014 Oct 8), 107113.
[61] J. Majdalani, C. Zhou, C.A. Dawson, Two-dimensional viscous flow between slowly expanding or contracting walls with weak permeability, J. Biomech. 35 (10) (2002 Oct 1) 1399–1403.